Published in final edited form as:
Cancer Res. 2010 August 1; 70(15): 6277–6282. doi:10.1158/0008-5472.CAN-09-4224.

Poly(ADP-ribose) polymerase inhibitor induces accelerated senescence in irradiated breast cancer cells and tumors

Elena V. Efimova[1,2,*], **Helena J. Mauceri**[1,2,*], **Daniel W. Golden**[1,2], **Edwardine Labay**[1,2], **Vytautas P. Bindokas**[3], **Thomas E. Darga**[1,2], **Chaitali Chakraborty**[1], **Juan Camilo Barreto Andrade**[1], **Clayton Crawley**[1], **Harold G. Sutton**[1,2], **Stephen J. Kron**[1,4], and **Ralph R. Weichselbaum**[1,2]

[1] Ludwig Center for Metastasis Research, The University of Chicago, Chicago, IL, 60637, USA

[2] Department of Radiation and Cellular Oncology, The University of Chicago, Chicago, IL, 60637, USA

[3] Biological Sciences Division Integrated Light Microscopy Core Facility, The University of Chicago, Chicago, IL, 60637, USA

[4] Department of Molecular Genetics and Cell Biology, The University of Chicago, Chicago, IL, 60637, USA

Abstract

Persistent DNA double strand breaks (DSBs) may determine the anti-tumor effects of ionizing radiation (IR) by inducing apoptosis, necrosis, mitotic catastrophe or permanent growth arrest. Ionizing radiation (IR) induces rapid modification of megabase chromatin domains surrounding double strand breaks (DSBs) via poly-ADP-ribosylation, phosphorylation, acetylation, and protein assembly. The dynamics of these ionizing radiation-induced foci (IRIF) have been implicated in DNA damage signaling and DNA repair. As an IRIF reporter, we tracked relocalization of GFP fused to a chromatin binding domain of the checkpoint adapter protein 53BP1 after IR of breast cancer cells and tumors. To block DSB repair in breast cancer cells and tumors, we targeted poly(ADP-ribose) polymerase with ABT-888 (veliparib), one of several PARP inhibitors currently in clinical trials. PARP inhibition markedly enhanced IRIF persistence and increased breast cancer cell senescence both *in vitro* and *in vivo*, arguing for targeting IRIF resolution as a novel therapeutic strategy.

Keywords

DNA damage response; PARP; IRIF; ABT-888; veliparib

Introduction

Small molecules targeting cellular responses to DNA damage have long been considered an attractive strategy to improve the effectiveness of genotoxic cancer therapy (1). An early event in the DSB response is rapid recruitment and activation of PARP1, resulting in

Corresponding Author: Ralph R. Weichselbaum, Dept. Radiation and Cellular Oncology, 5841 S. Maryland Avenue, Chicago, IL 60637. Phone: 773-702-0817; Fax: 773-834-7233; rrw@radonc.bsd.uchicago.edu.
[*] these authors contributed equally

Disclosure of Potential Conflicts of Interest
No potential conflicts of interest are known.

polymerization of poly(ADP ribose) (PAR) onto PARP1 itself, histones and other proteins at DSBs, and in the recruitment of macroH2AX to sites of DNA damage to stimulate chromatin remodeling, and DNA repair (2–4). PARP activity is required for normal DNA damage tolerance. While most attention has been paid to their potential in targeting malignancies defective in homologous recombination (HR) (5), PARP inhibitors are also promising as sensitizers for genotoxic agents and IR (6,7).

Coincident with PARP1 recruitment, ATM-dependent phosphorylation of histone H2AX to form γH2AX at DSBs promotes further chromatin modifications and assembly of proteins at IRIF such as MRE11/RAD50/NBS1, MDC1, 53BP1, and BRCA1 (8,9). Tracking accumulation and dispersal of IRIF proteins offer complementary reporters for checkpoint signaling and repair.

Herein, by exploiting GFP fused to the chromatin-binding domain of 53BP1 as a live-cell imaging reporter for DSB repair, we monitored the effects of PARP inhibition on irradiated breast cancer cells both *in vitro* and *in vivo*. ABT-888 blocked IRIF resolution and cell proliferation, driving tumor cells toward accelerated senescence and suppressing tumor regrowth compared to IR alone.

Materials and Methods

Cell culture and constructs

GFP fused to the human 53BP1 IRIF binding domain (10) was cloned into the pLVX-Tight-Puro lentiviral vector (Clontech), transduced into the MCF7 Tet-On Advanced® cell line (Clontech) and cultured in high glucose DMEM (Invitrogen) with 10% Tet system-approved Fetal Bovine Serum (FBS, Clontech). MCF7 Tet-On Advanced® is certified by Clontech as derived from MCF7 (ATCC) by viral transduction and was used without further authentication. After induction for 48 h with 1 μg/ml doxycycline (Sigma), GFP-positive cells were sorted to establish a stable MCF7$^{\text{Tet-On}}$ GFP-IBD cell line.

Xenograft tumors

17β-estradiol pellets (1.7 mg, Innovative Research of America) were implanted in female athymic *nude* mice (Harlan) 7 d prior to subcutaneous injection of 1×10^7 cells MCF7$^{\text{Tet-On}}$ GFP-IBD cells in 100 μl PBS. Once tumors grew to 300 mm^3, 2 mg/ml doxycycline with 1% sucrose was added to the drinking water for 72 h prior to IR. Mice received 0.5 mg ABT-888 in water twice daily by oral gavage in the 48 h prior to IR and thereafter as indicated.

Live-cell IRIF imaging

Live-cell images were captured on an Olympus DSU spinning disk confocal microscope and back-thinned EMCCD camera controlled by Slidebook v4.2 software or Zeiss Axiovert 200M and The Hammatsu Orca ER FireWire digital monochrome camera controlled by OpenLab software. For IRIF imaging in tumors, we used a Leica SP5 Tandem Scanner Two-Photon Spectral Confocal System controlled by LAS-AF 2.0 software.

Additional Methods

Detailed methods regarding cell lines, shRNA knockdowns, qPCR gene expression analyses, BrdU incorporation, clonogenic assays, PI staining, *in vitro* PARP activity assays, quantification of foci number and size, immunofluorescence, and SA-β-Gal staining are reported in Supplemental Data.

Results and Discussion

A 53BP1 IRIF binding domain GFP reporter reveals IR dose-dependent foci persistence in living cells

γH2AX foci and 53BP1 localization to IRIF can serve as proxies for unrepaired DSBs and the DNA damage response (8). The functional elements of the 53BP1 IRIF binding domain are a dimerizing domain, paired Tudor domains that recognize the stable histone marks H4-diMeK20 and/or H3-diMeK79, and a nuclear localization signal (10,11). Cells lacking PARP activity display a delay in H2AX phosphorylation and persistence of γH2AX foci (12). 53BP1 binding at IRIF is partly dependent on H2AX phosphorylation and chromatin remodeling, also influenced by PARP activity. Thus, to examine PARP inhibitor effects on IRIF kinetics in living cells, we placed GFP fused to the 53BP1 IRIF binding domain (10) under tetracycline-inducible control (GFP-IBD, Fig. S1) in a lentiviral vector. We transduced MCF7 Tet-On Advanced® (MCF7$^{Tet\text{-}On}$, Clontech), a cell line derived from MCF-7, a p53-positive, caspase-3 negative, and apoptosis-resistant human breast cancer-derived cell line, that stably expresses the Tet-On Advanced transactivator.

Following induction with doxycycline, unirradiated MCF7$^{Tet\text{-}On}$ cells expressing inducible GFP-IBD (MCF7$^{Tet\text{-}On}$ GFP-IBD) display pan-nuclear fluorescence, with only rare nuclear foci (mean 0.4 ± 0.7/cell). Consistent with previous reports, the GFP-IBD reporter relocalizes within minutes after IR to form nuclear foci that colocalize with γH2AX, endogenous 53BP1 and MDC1 proteins (Fig. S2). The GFP-IBD foci then slowly resolve over the next 24 h. The ATM kinase inhibitors KU-55933 and CGK733 decreased GFP-IBD foci formation (data not shown). In turn, shRNA knockdown of proteins required for 53BP1 re-localization to IRIF including ATM, MDC1, and RNF8 blocked formation of GFP-IBD foci after IR (Fig. 1*A*). Significantly, knockdown of endogenous 53BP1 increased the number of GFP-IBD foci in unirradiated cells and slowed their resolution after IR, indicating that 53BP1 remains active in MCF7$^{Tet\text{-}On}$ GFP-IBD cells.

We examined IRIF formation and resolution in relation to IR dose and time in MCF7$^{Tet\text{-}On}$ GFP-IBD cells *in vitro* (Fig. 1*B*, *C*). Most GFP-IBD foci resolve by 24 h at doses up to 8 Gy. For 2 Gy, the mean of 47 ± 13 IRIF at 3 h decreased to 3.2 ± 1.7 at 24 h, while for 8 Gy, the mean of 55 ± 15 IRIF at 3 h decreased to 12 ± 6 at 24 h. After 12 Gy, the mean of 53 ± 14 IRIF at 3 h decreased only to 37 ± 18 at 24 h. The increased IRIF persistence with higher IR dose suggests saturation of repair capacity or other damage responses. Indeed, doses above 6 Gy had greater effects on clonogenicity, a likely consequence of persistent DNA damage (Fig. 1*D*).

PARP1 inhibitor ABT-888 markedly enhances IRIF persistence, suppressing cell proliferation

Treating MCF7$^{Tet\text{-}On}$ GFP-IBD cells with IR in the presence of the PARP1 inhibitor ABT-888 (veliparib, 2-[(R)-2-methylpyrrolidin-2-yl]-1H-benzimidazole-4-carboxamide (13)) prevented PARP activation (Fig. S3) and markedly increased residual IRIF at 3 and 24 h (Fig. 2*A*, *B*). Neither the GFP-IBD reporter nor ABT-888 appeared to alter γH2AX localization or the recruitment of MDC1 and endogenous 53BP1 to IRIF (Fig. 2*B*). Time-lapse live-cell imaging of GFP-IBD revealed that in cells treated with 6 Gy, IRIF appeared within 15 min and began to decrease noticeably by 60 min (Fig. 2*C*,S4). However, after 6 Gy + ABT-888, IRIF continued to appear up to 60 min, perhaps via conversion of SSBs to DSBs (7), but remained largely unchanged thereafter. Previous data suggest that the growth of IRIF might maintain DNA damage signaling from unrepaired DSBs (14). While the mean size of IRIF formed in cells treated with ABT-888 was clearly smaller (Fig. S5), the total

volume of IRIF per cell at 24 h for IR + ABT-888 (187 ± 11/μm^3) was significantly greater than for IR alone (87 ± 10/μm^3, P = 0.005, *t* test).

ABT-888 alone slightly decreased colony formation at 10 μM (100 ± 1% for control *vs*. 88 ± 0.6% for ABT-888), but significantly reduced colony formation following 2 Gy (29.7 ± 1.5% for IR alone *vs*. 11.3 ± 0.6% for IR + ABT-888, P < 0.001, *t*-test), with similar fold reductions at each IR dose up to 6 Gy. We next examined potential mechanisms of growth suppression after IR + ABT-888. PARP inhibition did not dramatically affect MCF7$^{Tet\text{-}On}$ GFP-IBD cell death after IR. Even 7 days later, few cells exhibited propidium iodide permeability, suggesting that PARP inhibition might induce MCF7$^{Tet\text{-}On}$ GFP-IBD cell cycle arrest rather than apoptosis or necrosis. This is consistent with the previous observation that inhibition of ADP-ribosylation could block apoptosis, and a transient burst of PARP activity was required for apoptosis (15). Indeed, while ABT-888 alone did not appreciably decrease proliferating cells at 24 h (58 ± 1% BrdU$^+$ for control *vs*. 56 ± 1% for ABT-888, not shown), the anti-proliferative effects of 3 Gy (41 ± 1%) were enhanced by ABT-888 (27 ± 1%). In turn, MCF7$^{Tet\text{-}On}$ GFP-IBD cells treated with 3 or 6 Gy alone demonstrated a higher recovery of proliferative capacity compared to IR + ABT-888 (Fig. 2*D*).

ABT-888 accelerates senescence in irradiated MCF7$^{Tet\text{-}On}$ GFP-IBD cells *in vitro*

Unrepaired DNA damage can promote accelerated or premature senescence, even in cells with otherwise unlimited proliferative capacity (16–18). Accelerated senescence following IR has been observed in MCF7$^{Tet\text{-}On}$ GFP-IBD cells both *in vitro* and *in vivo* (19,20). At 4 d after IR + ABT-888, cells displaying persistent GFP-IBD foci began to exhibit morphology characteristic of senescence. At 7 d, surviving cells remained adherent, became enlarged with a flat morphology, and displayed multiple nuclear GFP-IBD foci (Fig. 3*A*). We investigated other hallmarks of accelerated senescence (16,17), including SA-βGal staining (Fig. 3*B*) and increased expression of the CDK inhibitor p21$^{Cip1/WAF1}$ (Fig. 3*C*). After 6 Gy + ABT-888, 76 ± 4% of surviving cells demonstrate SA-βGal staining compared to 1.2 ± 1.0% for ABT-888 and 2.5 ± 2.0% for 6 Gy (P < 0.001) and p21$^{Cip1/WAF1}$ gene expression was significantly upregulated following IR + ABT-888 compared to IR alone (P < 0.02, *t*-test). Immunocytochemistry suggested that the accumulation of p21$^{Cip1/WAF1}$ was greatest in cells with persistent IRIF (Fig. 3*D*). Accelerated senescence following IR and ABT-888 treatment is not limited to cells with wildtype p53, as we observed the same phenotype in MCF7$^{Tet\text{-}On}$ GFP-IBD cells treated with p53 inhibitor Pifithrin (data not shown) as well as in breast and other cancer cell lines with mutations in p53 (Fig. S6).

ABT-888 accelerates senescence and suppresses growth of irradiated MCF7$^{Tet\text{-}On}$ GFP-IBD tumors

To visualize IRIF *in vivo*, MCF7$^{Tet\text{-}On}$ GFP-IBD cells were injected into *nude* mice to form xenograft tumors. Imaging of GFP-IBD by two-photon microscopy revealed that the kinetics of IRIF formation and resolution in tumors were comparable to that observed in MCF7$^{Tet\text{-}On}$ GFP-IBD cells *in vitro* (Fig. 4*A*). When mice were treated with ABT-888 twice daily for 2 d prior to IR, and then twice daily thereafter, we observed no increase in IRIF number at early time points but the number of cells with residual IRIF increased at 24 h. 22% of tumor cells treated with 3 Gy exhibited ≥ 4 IRIF/cell while 42% of tumors cells with 3 Gy + ABT-888 had ≥ 4 IRIF/cell (P < 0.001, *t*-test, Fig. 4*B*). To evaluate DNA damage-induced senescence *in vivo*, we examined SA-βGal staining in frozen tumor sections at 7 d (Fig. 4*C*). ABT-888 alone slightly enhanced SA-βGal staining above background but markedly increased staining when combined with IR. To compare *in vivo* growth delay with that observed *in vitro*, we performed a tumor regrowth experiment. Mice bearing MCF7$^{Tet\text{-}On}$ GFP-IBD tumors were treated with ABT-888 for 2 d before a single 6 Gy dose, then only for 2 d after

IR. This short course of PARP inhibition significantly slowed MCF7$^{Tet\text{-}On}$ GFP-IBD tumor regrowth compared with 6 Gy alone (day 9, P = 0.021, day 12, P = 0.013, day 14, P = 0.001, *t*-test, Fig. 4*D*).

Our data confirm previously reported enhancement of IR effects by PARP inhibition (6,11) and implicate IRIF persistence as a potential mechanism of accelerated tumor cell senescence. Persistent cell cycle arrest and accelerated senescence are ascribed to accumulation of unrepaired DNA damage and chromatin perturbation, among other inducers (17,18). We speculate that the efficacy of PARP inhibitors toward homologous recombination deficient BRCA1, BRCA2 or PTEN negative cancer (21) may similarly reflect a cellular response to accumulation of unrepaired endogenous DNA damage. Indeed, preliminary analysis of the PTEN mutant cell line PC-3 suggests ABT-888 accelerates senescence, particularly in combination with radiation. While it remains dogma that IR and genotoxic agents mediate their lethal effects via enhanced apoptosis, necrosis or mitotic catastrophe, senescence is an alternative terminal phenotype that may be highly relevant as a determinant of outcomes for cancer treatment (16,22,23). Alone or in combination with other epigenetic drugs such as histone deacetylase inhibitors that promote IRIF persistence and accelerated senescence (24), PARP inhibitors may have a significant impact by inducing senescence as a novel mechanism for sensitization to radiation and chemotherapy.

Supplementary Material

Refer to Web version on PubMed Central for supplementary material.

Acknowledgments

Financial support: This research was supported by The University of Chicago Ludwig Center for Metastasis Research, the Foglia Family Foundation, The University of Chicago Comprehensive Cancer Center and NIH grants CA138365 and GM60443.

We acknowledge T. Halazonetis for generously providing reagents, and M. Pejovic, R. Torres and S. Bond for assistance.

References

1. Ljungman M. Targeting the DNA damage response in cancer. Chem Rev 2009;109:2929. [PubMed: 19545147]
2. Schreiber V, Dantzer F, Ame JC, de Murcia G. Poly(ADP-ribose): novel functions for an old molecule. Nat Rev Mol Cell Biol 2006;7:517–28. [PubMed: 16829982]
3. Gagne JP, Isabelle M, Lo KS, et al. Proteome-wide identification of poly(ADP-ribose) binding proteins and poly(ADP-ribose)-associated protein complexes. Nucleic Acids Res 2008;36:6959–76. [PubMed: 18981049]
4. Kraus WL. New functions for an ancient domain. Nat Struct Mol Biol 2009;16:904–7. [PubMed: 19739287]
5. Rodon J, Iniesta MD, Papadopoulos K. Development of PARP inhibitors in oncology. Expert Opin Investig Drugs 2009;18:31–43.
6. Donawho CK, Luo Y, Penning TD, et al. ABT-888, an orally active poly(ADP-ribose) polymerase inhibitor that potentiates DNA-damaging agents in preclinical tumor models. Clin Cancer Res 2007;13:2728–37. [PubMed: 17473206]
7. Liu X, Shi Y, Guan R, et al. Potentiation of Temozolomide Cytotoxicity by Poly (ADP) Ribose Polymerase Inhibitor ABT-888 Requires a Conversion of Single-Stranded DNA Damages to Double-Stranded DNA Breaks. Mol Cancer Res 2008;6:1621. [PubMed: 18922977]
8. Bonner WM, Redon CE, Dickey JS, et al. GammaH2AX and cancer. Nat Rev Can 2008;8:957–67.
9. van Attikum H, Gasser SM. Crosstalk between histone modifications during the DNA damage response. Trends Cell Biol 2009;19:207–17. [PubMed: 19342239]

10. Huyen Y, Zgheib O, Ditullio RA Jr, et al. Methylated lysine 79 of histone H3 targets 53BP1 to DNA double-strand breaks. Nature 2004;432:406–11. [PubMed: 15525939]
11. Pryde F, Khalili S, Robertson K, et al. 53BP1 exchanges slowly at the sites of DNA damage and appears to require RNA for its association with chromatin. J Cell Sci 2005;118:2043–55. [PubMed: 15840649]
12. Albert JM, Cao C, Kim KW, et al. Inhibition of poly(ADP-ribose) polymerase enhances cell death and improves tumor growth delay in irradiated lung cancer models. Clin Cancer Res 2007;13:3033–42. [PubMed: 17505006]
13. Penning TD, Zhu GD, Gandhi VB, et al. Discovery of the Poly(ADP-ribose) polymerase (PARP) inhibitor 2-[(R)-2-methylpyrrolidin-2-yl]-1H-benzimidazole-4-carboxamide (ABT-888) for the treatment of cancer. J Med Chem 2009;52:514–23. [PubMed: 19143569]
14. Yamauchi M, Oka Y, Yamamoto M, et al. Growth of persistent foci of DNA damage checkpoint factors is essential for amplification of G1 checkpoint signaling. DNA Repair (Amst) 2008;7:405–17. [PubMed: 18248856]
15. Simbulan-Rosenthal CM, Rosenthal DS, Iyer S, Boulares AH, Smulson ME. Transient poly(ADP-ribosyl)ation of nuclear proteins and role of poly(ADP-ribose) polymerase in the early stages of apoptosis. J Biol Chem 1998;273:13703–12. [PubMed: 9593711]
16. Roninson IB. Tumor cell senescence in cancer treatment. Cancer Res 2003;63:2705–15. [PubMed: 12782571]
17. Campisi J, d'Adda di Fagagna F. Cellular senescence: when bad things happen to good cells. Nat Rev Mol Cell Biol 2007;8:729–40. [PubMed: 17667954]
18. d'Adda di Fagagna F. Living on a break: cellular senescence as a DNA-damage response. Nat Rev Can 2008;8:512–22.
19. Chang BD, Broude EV, Dokmanovic M, et al. A senescence-like phenotype distinguishes tumor cells that undergo terminal proliferation arrest after exposure to anticancer agents. Cancer Res 1999;59:3761–7. [PubMed: 10446993]
20. Gewirtz DA, Holt SE, Elmore LW. Accelerated senescence: an emerging role in tumor cell response to chemotherapy and radiation. Biochem Pharmacol 2008;76:947–57. [PubMed: 18657518]
21. Mendes-Pereira AM, Martin SA, Brough R, et al. Synthetic lethal targeting of PTEN mutant cells with PARP inhibitors. EMBO Mol Med 2009;1:315–22. [PubMed: 20049735]
22. Lleonart ME, Artero-Castro A, Kondoh H. Senescence induction; a possible cancer therapy. Mol Cancer 2009;8:3. [PubMed: 19133111]
23. Collado M, Serrano M. Senescence in tumours: evidence from mice and humans. Nat Rev Can 2010;10:51–7.
24. Camphausen K, Burgan W, Cerra M, et al. Enhanced radiation-induced cell killing and prolongation of gammaH2AX foci expression by the histone deacetylase inhibitor MS-275. Cancer Res 2004;64:316–21. [PubMed: 14729640]

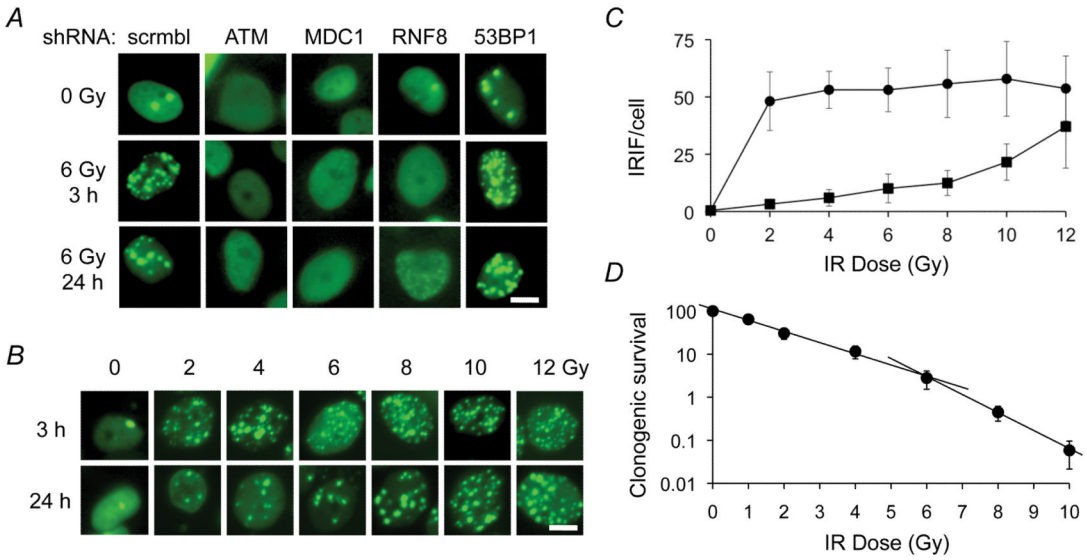

Figure 1.

GFP-IBD reporter reveals IRIF formation and kinetics. *A*, shRNA knockdown of the upstream DNA damage response protein ATM, MDC1 or RNF8 abrogates GFP-IBD reporter relocalization to IRIF. shRNA knockdown of endogenous 53BP1 increases foci numbers at 3 and 24 h. Scale bar, 10 μm. *B*, Formation and resolution of GFP-IBD foci in response to IR depend on time and dose. Scale bar, 10 μm. *C*, Mean number of GFP-IBD foci per cell ± SD (n > 50) at increasing IR doses evaluated at 3 h (*solid circles*) and 24 h (*solid squares*). *D*, Clonogenic survival of MCF7$^{\text{Tet-On}}$ GFP-IBD cells treated with increasing doses of IR (means ± SD, $n = 3$). Clonogenicity is modeled as distinct regimes of lower lethality from 0 to 6 Gy (% survival = $330 \times e^{-0.89 \text{ x (dose in Gy)}}$, $R^2 = 0.958$) and higher lethality from 6 to 12 Gy (% survival = $20.0 \times e^{-1.99 \text{ x (dose in Gy)}}$, $R^2 = 0.999$). Clonogenic efficiency of untreated MCF7$^{\text{Tet-On}}$ GFP-IBD cells represents 100% control.

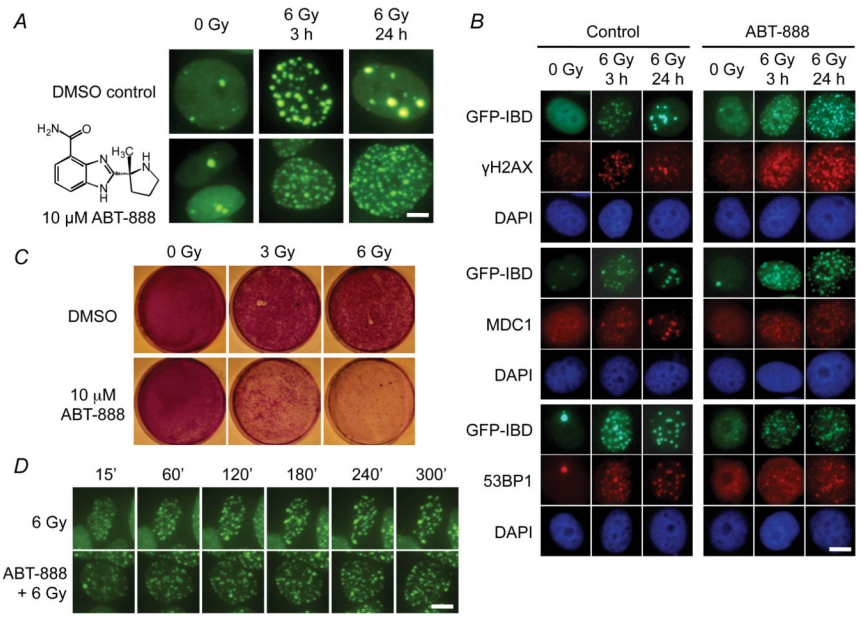

Figure 2.

PARP1 inhibitor ABT-888 (veliparib) alters IRIF dynamics and suppresses cell proliferation. *A*, ABT-888 increased the number of residual IRIF 24 h after IR. Cells were pretreated with DMSO (control) or 10 μM ABT-888 (inset) for 30 min before IR. Live cell images shown at 3 h and 24 h. Scale bar, 5 μm. *B*, Immunofluorescence reveals co-localization of GFP-IBD with γH2AX, MDC1, and endogenous, full-length 53BP1 at IRIF in cells treated with 6 Gy ± ABT-888. Nuclei indicated by DAPI staining (blue). Scale bar, 10 μm. *C*, Time-lapse live cell imaging of GFP-IBD localization in MCF7$^{Tet\text{-}On}$ GFP-IBD cells treated with 6 Gy ± ABT-888. Scale bar, 10 μm. *D*, ABT-888 suppresses cell growth of irradiated MCF7$^{Tet\text{-}On}$ GFP-IBD cells. Cells were treated as shown, fixed at 10 d and stained with crystal violet.

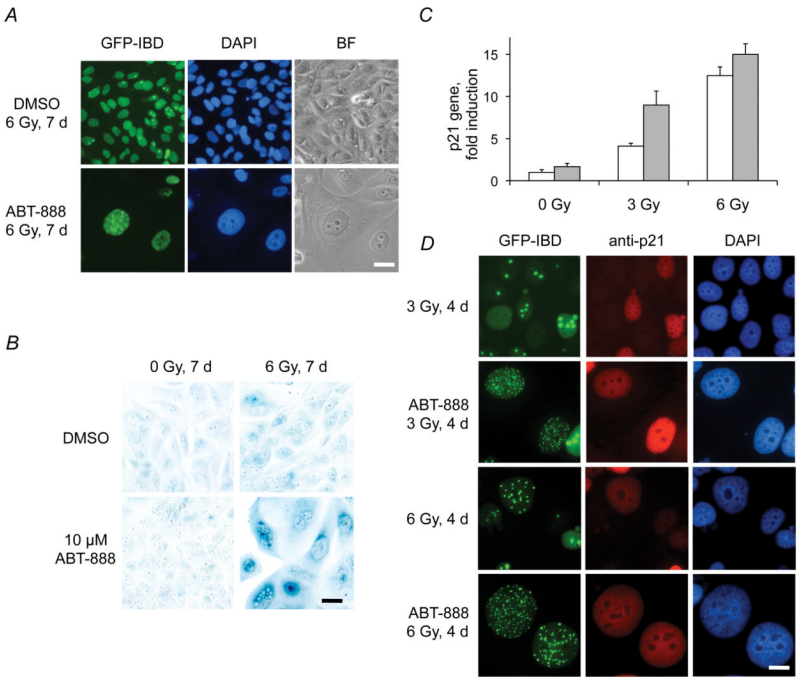

Figure 3.

ABT-888 induces accelerated senescence in irradiated MCF7$^{Tet\text{-}On}$ GFP-IBD cells. *A*, MCF7$^{Tet\text{-}On}$ GFP-IBD cells treated with IR + ABT-888 display persistent IRIF and develop senescent morphology. Scale bar, 20 μm. *B*, IR + ABT-888 increases SA-βGal activity. Cells were treated with 6 Gy ± ABT-888, fixed at 7 d and stained. Scale bar, 20 μm. *C*, Relative p21$^{Cip1/WAF1}$ transcript levels after IR ± ABT-888 determined by qPCR (mean ± SD, IR, white bars; IR + ABT-888, grey bars). *D*, Immunofluorescence staining for p21$^{Cip1/WAF1}$ at 4 d after 3 Gy ± ABT-888. Scale bar, 20 μm.

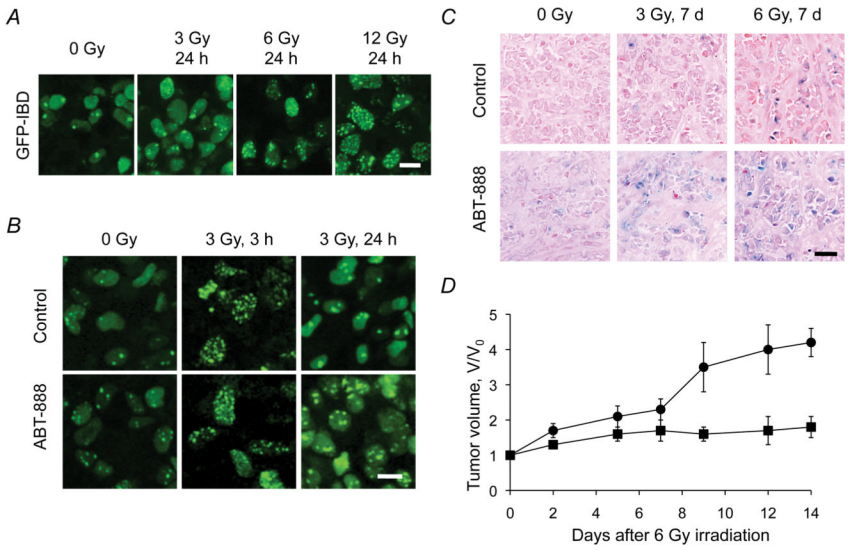

Figure 4.

IR + ABT-888 induces persistent IRIF and senescence *in vivo* and suppresses MCF7$^{Tet\text{-}On}$ GFP-IBD tumor regrowth. *A*, Dose-response of IRIF formation in xenograft tumor cells 24 h after IR. Scale bar, 10 μm. *B*, IR + ABT-888 increases residual IRIF compared to IR alone. Intravital imaging of GFP-IBD foci in tumors at 3 and 24 h after 3 Gy ± ABT-888. Scale bar, 10 μm. *C*, SA-βGal activity in tumors treated with IR ± ABT-888. Frozen sections of excised tumors 7 d after IR were fixed and stained. Scale bar, 20 μm. *D*, ABT-888 + IR suppresses tumor regrowth. Tumor growth was significantly delayed after 6 Gy + ABT-888 (*solid squares*) compared to 6 Gy (*solid circles*). Data graphed as mean fractional volume (V/V_o) ± SEM (n = 4/group).